ACS OMEGA

Open Access

http://pubs.acs.org/journal/acsodf

Article

Addressing the Effectiveness and Molecular Mechanism of the Catalytic CO_2 Hydration in Aqueous Solutions by Nickel Nanoparticles

Alessandro Sinopoli,* Ziao Liu, Ahmed Abotaleb, Alaa Alkhateeb, and Ivan Gladich*

Cite This: *ACS Omega* 2024, 9, 771−780

Read Online

ACCESS | Metrics & More | Article Recommendations | Supporting Information

ABSTRACT: Hydration of carbon dioxide in water solution is the rate limiting step for the CO_2 mineralization process, a process which is at the base of many carbon capture and utilization (CCU) technologies aiming to convert carbon dioxide to added-value products and mitigate climate change. Here, we present a combined experimental and computational study to clarify the effectiveness and molecular mechanism by which nickel nanoparticles, NiNPs, may enhance CO_2 hydration in aqueous solutions. Contrary to previous literature, our kinetic experiments recording changes of pHs, conductivity, and dissolved carbon dioxide in solution reveal a minimal effect of the NiNPs in catalyzing CO_2 hydration. Our atomistic simulations indicate that the Ni metal surface can coordinate only a limited number of water molecules, leaving uncoordinated metal sites for the binding of carbon dioxide or other cations in solution. This deactivates the catalyst and limits the continuous re-formation of a hydroxyl-decorated surface, which was a key chemical step in the previously suggested Ni-catalyzed hydration mechanism of carbon dioxide in aqueous solutions. At our experimental conditions, which expand the investigation of NiNP applicability toward a wider range of scenarios for CCU, NiNPs show a limited catalytic effect on the rate of CO_2 hydration. Our study also highlights the importance of the solvation regime: while Ni surfaces may accelerate carbon dioxide hydration in water restricted environments, it may not be the case in fully hydrated conditions.

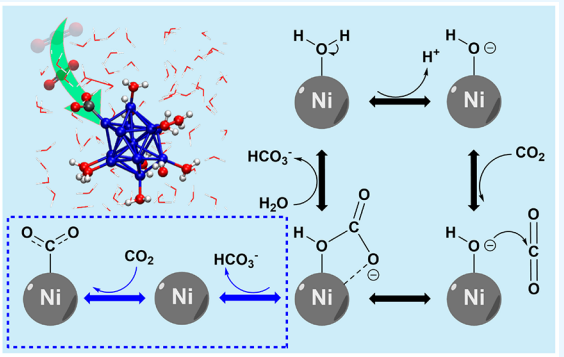

INTRODUCTION

Carbon dioxide is a greenhouse gase (GHS) and considered one of the main ones responsible for the increment of the average global temperature and, hence, the rising of sea level and the ocean acidification.[1,2] The 2015 Paris agreement sets a global effort to hamper the increase of the global average temperature,[3] but this does not come without obstacles since CO_2 is a byproduct of combustion processes, needed to satisfy the energy demand of our modern world. Among the plethora of technologies that could help in mitigating climate change and reducing the levels of GHS, carbon capture and utilization (CCU) certainly represents one of the most promising CO_2-based technologies. In the industrial sector, postcombustion CO_2 capture is heavily practiced, generally using traditional amine-based scrubbing solutions, but the amine regeneration still remains an energetically expensive step.[4,5] In CCU processes, carbon dioxide is converted into added-value products, such as carbonates and methanol,[6,7] reducing the overall capture operating cost. For example, mineralization of captured CO_2 into carbonates is an eco-friendly and economically appealing CCU technology since carbonates can be reused in the construction industry and beyond.[8,9] In the mineralization process, carbon dioxide, from sources such as flue gas, reacts with sources of alkaline metal ions (typically from group 2, e.g., Mg^{2+} and Ca^{2+}) to form stable solid carbonates (typically $MgCO_3$ and $CaCO_3$).

The majority of CCU technologies, mineralization included, play around the dissolution of carbon dioxide in solution and the corresponding pH-dependent equilibria between CO_2(aq), carbonic acid (H_2CO_3), bicarbonate ion (HCO_3^-), and carbonate ion (CO_3^{2-}).[10] Since the early studies dating back to 1912,[11] it is clear that hydration is the rate limiting step in the CO_2 mineralization process, as also confirmed by more recent experimental and computational studies.[12,13] In nature, CO_2 hydration reaction is catalyzed by carbonic anhydrase (CA), a zinc-based metalloenzyme able to accelerate the CO_2 hydration rate. CA has been successfully adopted,[14] but the cost of extraction of the enzyme and the specific range of operation (i.e., basic pH and low temperature of the solution) are limiting factors to its large scale application.[14,15] A huge research effort has been taken over the past years, designing

Received: September 5, 2023
Revised: December 5, 2023
Accepted: December 6, 2023
Published: December 26, 2023

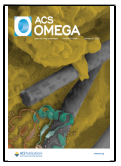

better solvents for carbon dioxide capture[16−18] and finding the more cost-effective catalysts that mimic the active site of CA, enabling the scaling-up of the chemical process at the industrial level.[18−26]

In 2013, the group of Siller at Newcastle University investigated the role of nickel particles in the formation of exoskeletons of sea urchin larvae, suggesting that nickel particles were able to absorb carbon dioxide and catalyze its transformation into calcium carbonates, the main component of animal shells.[27−29] Thus, nickel nanoparticles (NiNPs) would have accelerated CO_2 hydration reaction, as a first wholly inorganic heterogeneous catalyst for CO_2 hydration.[27−29] XPS results were employed to draw a hypothetical chemical mechanism for this catalytic process,[27] which is reported (in black) in Figure 1. When solvated, NiNPs

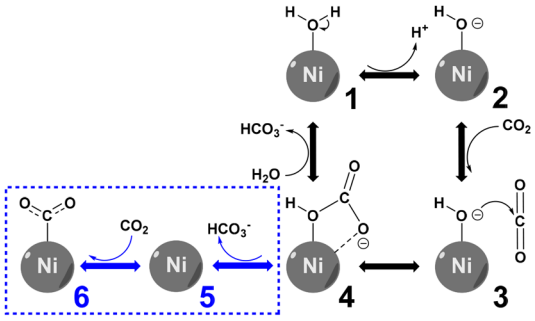

Figure 1. Schematic reaction mechanism of CO_2 hydration catalyzed by NiNPs, suggested in ref 27. The blue dashed line (steps 5 and 6) represents the new alternative pathway presented in this work.

coordinate and deprotonate water molecules on their metal surface, leading to the formation of a metal surface decorated by hydroxyl groups: these hydroxyl groups are then capable of capturing and hydrating CO_2 into surface-bound bicarbonate ions. Finally, the surface-bound bicarbonate would be replaced by another water molecule, releasing bicarbonate in the solution and re-forming a new Ni-surface coordinated hydroxyl group, enabling a next cycle of CO_2 capture and hydration.[27] Siller and co-workers employed NiNPs catalysts to obtain solid carbonate products from desalination brines in a tubular reactor using different pH-regulating approaches, without the need for an alkaline earth metals dissolution step.[30] More recent kinetic studies on planar organometallic Ni^{2+} complexes have shown that if an interfacial Ni−OH forms, it reacts rapidly with carbon dioxide, producing a carbonate Ni−OCO_2H species.[31] Recent ambient pressure XPS experiments[32] have reported the spectroscopic signature of water vapor adsorption on Ni surfaces, which catalyzes carbonate production on Ni(100) metal surface (but not on the Ni(111) surface).[32] Interaction between the nickel surface and CO_2 has been also computationally explored, reporting more favorable adsorption energies for a gas phase water molecule than for CO_2 on different metallic surfaces of Ni: for water the chemisorption energies ranged between −0.2 and −0.39 eV (depending on the Ni facets),[33] while for CO_2 it was −0.14 eV or even weaker binding for certain Ni surfaces.[34] These results seem to corelate with the mechanism suggested by Siller and co-workers in ref 27 with CO_2 conversion to bicarbonate ion occurring at the hydroxyl coordinated groups on the Ni surface.

While some works seem to support the mechanism suggested by Siller and co-workers, there is still not a general agreement on the catalytic effects of NiNPs on CO_2 hydration in solution, effect that has been questioned in the literature.[35,36] Bodor et al.[37] reported a marginal benefit using NiNPs for the capture, hydration, and follow-up mineralization of gas phase CO_2 using CaO and steelmaking slags as the source of Ca^{2+}, especially when the solid (slag) to liquid (reaction medium) ratio is high. This result was rationalized by the possibility that (a) Ca^{2+} dissolution, rather than the CO_2 hydration, is the rate limiting step or, alternatively, (b) when the solid to liquid ratio is high, the poisoning of the NiNP surface by a rapid covering of formed calcium carbonate, stopping the NiNP catalytic effect on the CO_2 hydration reaction. From a mechanistic point of view, the poisoning of the NiNP means that surface-bound carbonate is not released into the solution (i.e., from step 4 to step 1 in Figure 1), as it has been suggested previously,[28] but it rather sticks on the surface, deactivating the catalyst. It was concluded by Bodor et al. that to further accelerate the NiNP-assisted process, carbonation of solutions containing dissolved alkaline earth metals, such as brines and brackish waters, may benefit more from NiNP addition than those based on mineral carbonation dissolution. Along this line, recent experimental studies reported that monovalent cations or cationic polymer competes for the coordination on NiNp sites.[38] Density functional theory calculations have also shown that, at high H_2O coverage, water prefers to form water clusters by hydrogen bonds rather than coordinating with the Ni surface.[39] These studies may suggest that, contrary to what has been observed with the adsorption of few water vapor molecules,[33,34] cations (or CO_2 itself) may compete with water for the coordination with the Ni surface in bulk water solutions, deactivating the catalyst. Thus, the possibility to capture CO_2 (or other cations) on the NiNp surface implies the hampering of carbonate formation by reaction with surface hydroxyl coordinated groups (i.e., step 3 in Figure 1) or the existence of a different chemical pathway for carbonation that does not rely on the water coordination on the metal surface. It is worthy mentioning that, at the present date and to the best of our knowledge, the molecular picture of the process comes from computational studies in very limited hydration regime (i.e., one CO_2 and a single or a few water molecules adsorbed on the Ni surface)[32−34,39,40] due to the computational cost for proper modeling of metal/water interfaces.[41] A comprehensive molecular picture of the catalytic effects of NiNPs on CO_2 hydration in solution is hence still missing, which is also contributing to the questioning of the effectiveness of this process in bulk solution.

Motivated by the global R&D demand for the improvement of CCU at industrial scale, we present a combined experimental and computational study aiming to shine a light on the effectiveness and the molecular mechanism by which NiNP may enhance CO_2 hydration. The advantages of NiNPs may be several: they can be isolated magnetically from solutions and recycled, immobilized on silica supports,[42,43] they are economically more accessible, and they can work at room temperature and atmospheric pressure.[27] In the industrial setting, thanks to their high surface area, NiNPs could offer a potential alternative to carbonic anhydrase-based enzymes, which have limitations in terms of stability, pH and temperature range of applicability. We exploited kinetic experiments recording changes of pH, conductivity, and

https://doi.org/10.1021/acsomega.3c06676
ACS Omega 2024, 9, 771−780

dissolved CO_2, during CO_2 sparging in aqueous solution with and without the use of immersed NiNPs. We explored a set of different NiNP concentrations, also carefully controlling the experimental conditions (e.g., NiNP mixing in solution, Ni leaching, CO_2 pressure, etc.) and critically comparing our setup with those in the literature. Our experimental results indicate a negligible effect of NiNps in catalyzing the CO_2 hydration reaction. Our atomistic simulations based on *first principles* molecular dynamics of NiNp in bulk water clarify that when water coordinates with the metal surface, there is a charge transfer from the lone pair of the oxygen to the Ni surface, limiting the number of coordinated water molecules on the metal surface. Thus, in line with recent experimental and computational conclusions on water adsorption on the Ni surface in a limited hydration regime, the Ni surface cannot coordinate an unlimited number of water molecules: we here observe partial water decoordination from the Ni surface and water clustering by hydrogen bonding, leaving uncoordinated metal sites for the possible binding of carbon dioxide or cations in solution. The net effect is to deactivate the catalyst limiting the continuous re-formation of a hydroxyl-decorated surface, which is the key chemical step of the previously proposed Ni-catalyzed hydration process of CO_2 in Figure 1. Our computer simulations also report the same effect not only on NiNPs but also when water molecules are adsorbed on the 111 Ni slab interface, with the formation of water clustering on top of the metal surface. These clusters can form water cages around chemisorbed CO_2, enhancing Ni−CO_2 recombination and then the stability of the chemisorbed carbon dioxide (i.e., a solvent cage effect). To summarize, our experimental and computational results suggest (at least under our experimental conditions) a limited catalytic effect of NiNPs on CO_2 hydration in bulk solution. Moreover, we here highlight that the solvation regime is crucial for the effectiveness of the chemical process: while, in water-restricted environments, NiNPs can accelerate the CO_2 hydration, it may be not the case in fully hydrated conditions.

METHODS

Materials. Sodium hydroxide (pellets, NaOH, ≥98%) was purchased from Sigma-Aldrich, and nickel nanoparticles were purchased from Nanoshel LLC (U.K.), with a 40−60 nm range of diameter. In the carbonation experiments, CO_2 gas of 5 N purity was purged at pressure of 0.2 bar. For all of the experiments, deionized (DI) water was used. Sample solutions were prepared by adding 15 and 30 ppm, respectively, of NiNp to DI water, followed by 10 min of sonication.

Reaction Kinetics. To enhance the dissolution of CO_2 (as for example in a scrubbing solution) and to extend our knowledge on the applicability of NiNPs, the pH of the deionized (DI) water used for all of the experiments has been adjusted to a value range of 8.2−8.5 by addition of 1 M NaOH, prior to the injection of the NiNP. Indeed, as depicted in Figure 1 (reaction steps 1 and 2) the sole NiNP addition lowers the initial pH of the solution: this NaOH addition was necessary to increase the alkalinity of the solution, favoring CO_2 solubility in water, resembling common carbon capture practice by scrubbing solutions. In addition, we also performed the same CO_2 dissolution experiments without altering the initial pH with NaOH for DI water and 30 ppm NiNPs, respectively.

CO_2 hydration kinetics experiments were undertaken with a fixed volume of solution (100 mL) in a 250 mL automated jacketed reactor (Atlas by Syrris). Temperature was set to 21 °C. Solution was stirred at 300 rpm (by nonmagnetic propeller) for 30 min prior to CO_2 sparging for a further 30 min at a pressure of 0.2 bar. The pH and conductivity were continuously measured using pH and temperature probe integrated in the automated reactor. Before and after the carbonation experiments, Inductively coupled plasma (ICP) analysis, by Agilent 5800 ICP-OES, was used to determine the concentration of Ni^{2+}. The dissolved CO_2 was monitored by a CO_2 Sensor InPro5000i (Mettler Toledo). For each NiNP concentration, all reaction kinetics were repeated three times and a statistical error bar has been assigned to average profiles of pH, hydronium ion concentration, and conductivity. A schematic picture of the experimental apparatus is reported in the Supporting Information, Figure S1.

Dissolved CO_2 Measurement. A set of reactions with DI water and 15 and 30 ppm NiNPs has been performed to monitor the dissolved CO_2 with a dedicated probe. The dissolved CO_2 sensor was based on the Severinghaus principle which utilizes the correlation between dissolved CO_2 and pH of a liquid. The potentiometric Severinghaus electrode utilizes a bicarbonate buffer system in contact with the measured medium through a selective CO_2-permeable membrane. The pH value in the buffer system is related to the partial pressure of dissolved CO_2 present in the process media. The CO_2 from the medium diffuses across the membrane until it equilibrates within the buffer solution. A change in the CO_2 partial pressure results in a pH change in the electrolyte, which is detected by the inner body pH electrode.

Computational Modeling. Atomistic computer simulations of nickel nanoparticles (NiNPs) in aqueous solution were performed using an icosahedral particle of 13 Ni atoms: this structure consists of 1 inner atom and 12 atoms exposed to the liquid phase. The icosahedral structure was selected as a proxy of our experimental nanoparticle because its structure has been characterized in the literature,[44] and its limit size made possible to perform accurate first principles molecular dynamics simulation at a reasonable computational cost. Our icosahedral particle exposes 12 vertices to the liquid phase, which are prone to CO_2 and water adsorption.

The NiNP was geometrically optimized in vacuum, resulting in a Ni−Ni bond of 2.56 Å, very close to the one reported in literature.[44] Afterward, the structure was coordinated with 12 water molecules, one for each vertex (Figure S2) and further optimized in a vacuum. The coordinated NiNP was then solvated in a 15.2 Å side cubic box of 89 water molecules and one CO_2, for a final simulation box of 101 water molecules, 1 CO_2 and 13 Ni atoms. Constant pressure and temperature (i.e., *NPT* ensemble) molecular dynamics (MD) simulations were finally performed, allowing the simulation box to adjust to the applied pressure. The simulation box size reached equilibration after 250 fs.

A 2D Ni slab exposing its 111 interfaces to the vacuum phase was created starting from a face-centered Ni bulk crystal structure downloaded from material project (mp-23).[45,46] The vacuum/Ni(111) interface has been chosen because it has been proven experimentally and computationally to be the most stable one.[39,47] The slab comprises 144 Ni atoms, with a lateral dimension of ∼15 Å × 13 Å in the *XY* dimension and 4 Ni layers in the *Z* direction (i.e., the 111 direction). The *Z*-direction of the simulation box was enlarged to 40 Å, resulting in the formation of two vacuum/Ni interfaces. Figure S3 shows snapshots of the Ni slab structure. After a geometry

https://doi.org/10.1021/acsomega.3c06676
ACS Omega 2024, 9, 771−780

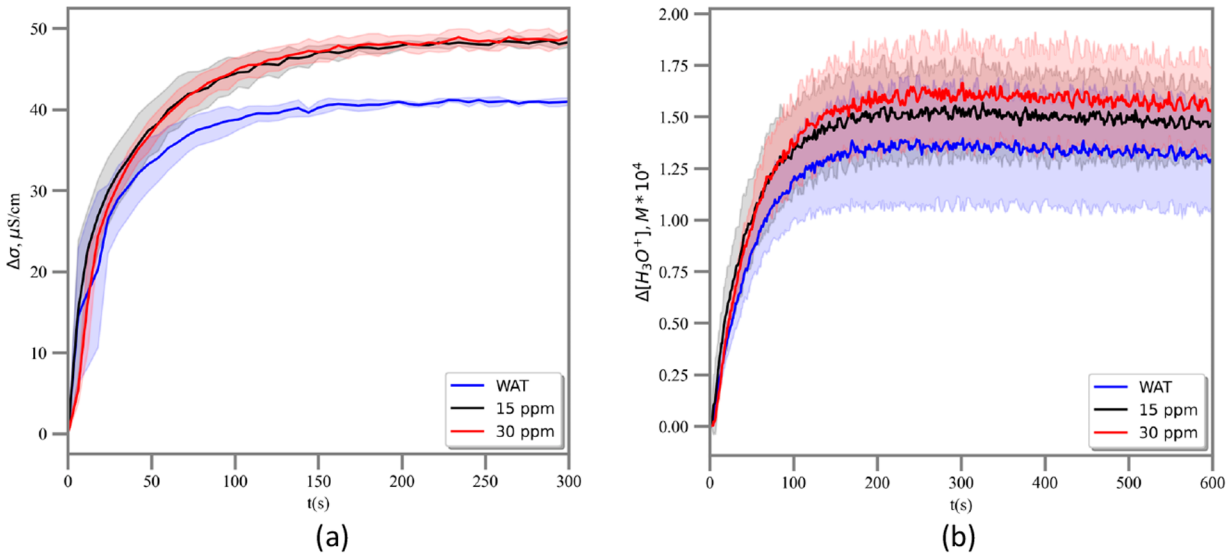

Figure 2. Effect of adding NiNPs to DI water on the CO_2 hydration. (a) Difference, $\Delta\sigma = \sigma_{(t)} - \sigma_{(t=0)}$, between conductivity at time t and at $t = 0$. (b) Difference, $\Delta[H_3O^+] = [H_3O^+]_{(t)} - [H_3O^+]_{(t=0)}$, between H_3O^+ concentration at time t and at $t = 0$. $t = 0$ corresponds to the starting time of CO_2 bubbling in solution. In both panels a and b, shadow regions correspond to one standard deviation confidence interval, calculated over three different measurements for each NiNP concentration.

optimization of the structures, (a) 6 water molecules or (b) 12 water molecules and 1 CO_2 were placed on one of the two 111 surfaces, before performing a further geometry optimization by energy minimization at density functional theory level.

All of the simulations were performed at first principles level (FPMD), i.e., the forces governing the dynamics of the system were calculated *on-the-fly* by employing density functional theory (DFT). Here, we exploited two different FPMD simulations, one using PBE[48,49] and another using RPBE[50] density functional theory in combination with Grimme's dispersion correction (D3).[51] Both DFT methods were used in literature to study gas phase CO_2 and water adsorption on different Ni facets.[32,34,39] Valence electron were treated by DZVP basis set along with plane wave representation truncated at 500 Ry, while Goedecker-Teter-Hutter pseudopotential[52] were used to model core electrons. The time step was set to 0.5 fs. The temperature was kept at 300 K and the pressure at 1 bar using a Nose-Hoover thermostat and barostate, respectively, with a time constant of 50 fs.[53] CP2K molecular dynamic package was exploited to run all the FPMDs.[54] The Fermi−Dirac smearing scheme implemented in CP2K,[54] with an electronic temperature of 2000 K, was adopted to treat the electron population of the spin channels. All calculations were performed under full 3D periodic boundary conditions.

The bond formation between water (or CO_2) and the surface of the NiNP was tracked by calculating the coordination number, CN, between the surface Ni atoms and the water oxygen (or the carbon atom of CO_2), using a cutoff distance of 0.25 nm for the water oxygen−Ni distance and 0.22 nm for the C−Ni one. The coordination number CN is constructed by employing a smooth switching function of the atomic distance: when the distance of the two atoms is below a cutoff distance, the CN assumes a value of ∼0.9; above the cutoff distance, CN goes to zero. CN is a convenient and quantitative parameter to check whenever a bond is formed (CN ≥ 0.9), whether the bond between two atoms is broken but the atoms are still in contact with the first solvation shell (CN ∼ 0.2) or if they went far apart (CN ∼ 0). PLUMED plug-in was used for the postprocessing and analysis.[55]

RESULTS AND DISCUSSION

To evaluate the effectiveness of nickel nanoparticles on CO_2 hydration, we performed carbonation experiments on DI water at different nanoparticle concentrations. Here, we considered 15 and 30 ppm concertations, respectively.[27] The rationale behind this concentration choice was to test the effectiveness of the NiNPs addition at the fastest rate (i.e., 30 ppm)[27] and at a lower concentration (i.e., 15 ppm), to verify the minimum conditions to observe a catalytic effect. Upon bubbling of CO_2 into the aqueous solution, the expected reactions are

$$CO_2(gas) \rightarrow CO_2(aq) \quad (1)$$

$$CO_2(aq) + 2H_2O \leftrightarrow HCO_3^- + H_3O^+ \quad (2)$$

We conducted measurements of the solution conductivity as a function of time, which are reported in Figure 2a. An increase in the solution conductivity provides a measurement of ion formation in solution. Before starting the bubbling of CO_2 into the aqueous solution, we observed that the sole addition of nickel NPs led to a minimum increase of the conductivity by an average of 2 μS/cm over the two NiNP concentrations considered here (i.e., 15 and 30 ppm) compared to DI water. This initial increase of the conductivity prior to any CO_2 bubbling is ascribed to both leached Ni^{2+} ions (discussed below) and to the fact that the sole addition of NiNPs decreased the initial pH values as consequence of an initial water coordination and deprotonation (i.e., formation of −OH groups) at the metal surface, as sketched in Figure 1 (steps 1 and 2). For this reason, Figure 2a reports the difference in conductivity, $\Delta\sigma$, between time t and $t = 0$, where $t = 0$ corresponds to the starting time of the CO_2 bubbling. After 10 min of sole stirring, CO_2 at 0.2 bar has been continuously sparged in the sample solutions (at time $t = 0$) and the conductivity been recorded.

https://doi.org/10.1021/acsomega.3c06676
ACS Omega 2024, 9, 771−780

Figure 2a shows that the conductivity increases with time, as the result of ion formation in solution, i.e., bicarbonate, hydronium, and (potential) Ni^{2+} from NiNP leaching. In the presence of NiNP, the final conductivity is ∼50 μS/cm, irrespective on the NiNP concentration in solution, a value higher than the one detected in DI water where the final $\Delta\sigma \sim$ 38 μS/cm. It is worthy remarking that in previous experiments presenting the catalytic activity of NiNP on the CO_2 hydration, no leaching of Ni was reported[27] and the conductivity was only associated with a generation of carbonates in solution according to reaction 2 and, thus, considered a proof of the catalytic activity of the NiNPs. On the other hand, we here observed by ICP analysis a concentration of approximately 100−300 ppb Ni^{2+} ions after the carbonation reactions. Therefore, we are not inclined to ascribe the larger final conductivity with NiNP than in pure DI water solely to a greater presence of carbonates and hydronium ion in solution but also to a contribution of leached Ni^{2+}. Moreover, in Figure 2a the conductivity seems not affected by the concentration of NiNPs in solution: this fact suggests that (a) the leaching of Ni^{2+} from the NiNPs to the solution reached an equilibrium already at 15 ppm and (b) a higher concentration of NiNPs does not enhance the concentration of hydronium and carbonates in water.

Figure 2b reports the concentration of hydronium ion calculated by recording the pH of the solution as a function of time, where t = 0 is again the start of the CO_2 bubbling in solution. As mentioned before, since the addition of NiNPs in solution lower the initial pH before bubbling, Figure 2b show the difference between the concentration of hydronium ion at time t, $[H_3O^+](t)$, and at the time of the CO_2 bubbling start, t = 0. In this way, the variation of hydronium ion concentration in Figure 2b refers to that generated by the chemical mechanism in reaction 2, and it is directly linked to the formation of carbonates in solution. We reported the raw pH versus time series in Figure S4. Figure 2b shows that the trend is slightly faster with NiNPs but not significantly because all of the profiles are within one standard deviation (i.e., the shadow region in Figure 2b). It is important to note that, in previous work,[27] the catalytic activity of the NiNPs in solution has been judged by looking at the pH as a function of time and not its relative difference to the initial value. Here, we do not see a significant acceleration of the reaction with NiNPs. To further support this statement, Figure S5 shows the rate calculated as the incremental ratio, i.e., the hydronium concentration difference between time t and t = 0, divided over time. Figure S5 reports faster kinetics with NiNP compared to the pure water case, but differences are very minimal. Finally, in our test experiments in the absence of NaOH, the effects of NiNPs on CO_2 hydration are still visible (Figure S6) but less pronounced than in Figure 2, stating that the initial pH adjustment by NaOH addition does not alter the conclusion about a limited catalytic effect of the NiNP on carbon dioxide hydration in aqueous bulk solution.

We recorded the dissolved CO_2 in a dedicated set of reactions with DI water and 15 and 30 ppm NiNPs. The intrinsic mechanism of the sensor (see Methods) generates a delay between the start of the reaction (i.e., t = 0, when CO_2 was started to be bubbled into the solution) and a measurable increase of dissolved CO_2 in solution. Indeed, as noted in Figure 3 the concentration of CO_2 starts increasing only after 60 s, whereas pH and conductivity (Figure 2) register an immediate variation. The curves for 15 and 30 ppm revealed an

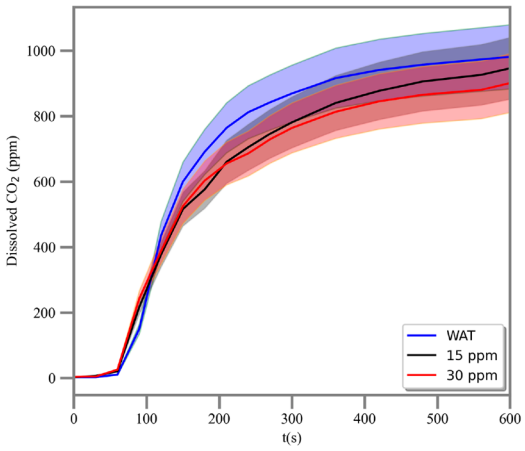

Figure 3. Dissolved CO_2 measurement. Shadow regions correspond to the confidence intervals of the measurements, calculated from the accuracy provided by the probe instrument (±10% of the detected value).

initial faster dissolution of CO_2, but after 110 s the concentration of CO_2 in the DI system overcomes the performance of NiNPs. Nevertheless, all curves tend to a plateau value after 10 min, a value that is approximately 1000 ppm for all three concentrations. Assuming an equilibrium after 10 min with a CO_2 concentration of 1000 ppm in aqueous solutions and using the equilibrium constant of the carbonic anhydrase in the absence of the catalyst, $K = 10^{-6.35}$ M,[56] the predicted amount of hydronium ions in solutions by reaction 2, is $1.1 \times 10^{\wedge-4}$ M, which well matches the values in Figure 2a, supporting both conclusions from pH and probed CO_2. Moreover, even if the CO_2 solubility depends on multiple factors in a not trivial relation (i.e., pH, ionic concentration, etc.),[57,58] our plateau value (∼1000 ppm) is in the range of those reported in literature at the same pH values.[58] The initial boost in the dissolved CO_2 (Figure 3) with NiNPs, together with the variation of hydronium concentration (Figure 2b) suggest the co-presence of multiple mechanisms when NiNPs are present in the solution, which are discussed below.

Atomistic simulations based on first principles molecular dynamics (FPMD) of an icosahedral NiNp in bulk water were performed to address the physicochemical behaviors of NiNPs in solution and to elucidate molecular mechanisms behind our experimental findings. Upon hydration in bulk water, FPMDs show that an initially 12 water coordinated NiNP optimized in vacuum (Figure S2) undergoes an almost instantaneous detachment of some of the coordinated water molecules from the metal surface, exposing some uncoordinated Ni sites to the liquid phase. After water desorption from the cluster surface, on one of the exposed vertexes, CO_2 gets chemisorbed (Figure 4). The water detachment and the CO_2 chemisorption processes occur quite rapidly within 2 ps. This is shown in Figure 4: CO_2 converts from the linear (gas phase) structure (Figure 4a) to the bent adsorbed structure (Figure 4b), which is a sign of the chemisorption event. Figure 4 shows results at the PBE density functional theory level. Similarly, the immediate detachment of water from the Ni surface was also observed in the FPMD simulation at the RPBE level (Figures S7 and S8), but in this case, due to the limited simulation time, CO_2 chemisorption was not observed. For both FPMDs at PEB and RPBE theory levels, we observe a distortion of the icosahedral structure upon immersion in solution.

https://doi.org/10.1021/acsomega.3c06676
ACS Omega 2024, 9, 771−780

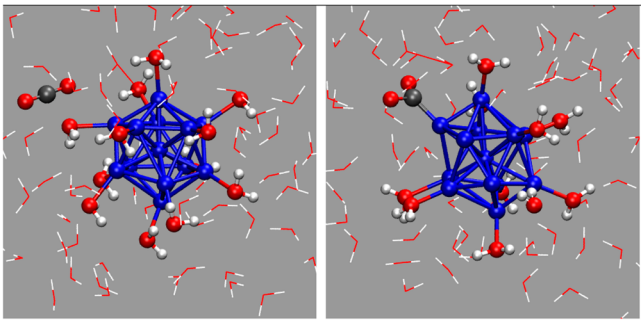

Figure 4. Snapshots from the FPMD trajectory at the PBE density functional theory level. (a) Starting configuration. (b) Structure after 2 ps simulation. Atom color code: O, red; Ni, blue; H, white. Ball and stick visualization for the CO_2 molecule and the NiNP and its coordinated water molecules. Other solvent (water) molecule in line representation.

The coordination number, CN, between the water molecules and Ni surface atoms enables a more quantitative analysis of the chemisorption process of CO_2. As mentioned in our methodology, the CN is ∼0.9 when two atoms are at a distance smaller than 0.25 nm (or 0.22 nm for the C−Ni one). For the initial NiNP coordinated with 12 water molecules, the CN between the water and Ni atoms, CN(Ni−O_w), fluctuates between 10 and 11, as shown in Figure 5a. After a short time (∼0.75 ps), CN(Ni−O_w) suddenly drops and oscillates around 9.5, a value which is consistent with the decoordination of 2 water molecules (of the 12 initially coordinated) from the metal surface. After 1 ps, the coordination of the CO_2 to the NiNp surface takes place, and the CN between Ni and C atom, i.e., C(Ni−C), jumps to ∼0.9 (Figure 5b). Figure 5c correlates the water desorption, and the resulting CO_2 coordination, with the total charge of the NiNP. The initial NiNp charge is −1.2 *e*; after water detachment the charge of the NiNP fluctuates at ∼−1.1 *e*, showing that there is an anticorrelation between water coordination and charge: when CN(Ni−O_w) is higher, the NiNP charge is lower, and vice versa. At 1 ps, CO_2 chemisorption occurs and the NiNP total charge jumps to ∼−0.8 *e* due to the electron donating character of the metal with respect to the carbon atom. The same picture can be drawn from results at RPBE FPMD (Figure S8), with the total NiNP charge and the CN(Ni−O_w) still anticorrelating.

To address the impact of a different surface/volume ratio or curvature of the NiNp particles on the hydration of carbon dioxide, we also performed simulations of gas-phase water and CO_2 adsorption on a 2D Ni slab. We focused our attention on the chemisorption of (a) 6 water molecules and (b) 12 water and 1 CO_2 on the 111 interface. Panels a and b of Figure 6 show the starting and final structures after 200 steps of geometry optimization, displaying the detachment of one water molecule from the Ni surface. This is quantitatively depicted in Figure 6c, showing the number of Ni−C bonds calculated as the coordination number (CN) divided by 0.9. Figure 6c shows an initial number of 6 coordinated water, but after ∼140 steps, one water detaches from the surface. Similar to Figure 5, also in Figure 6c,d we observe an increase in the Ni-slab charge upon water detachment. In the presence of more adsorbed water, Figure 7 indicates the formation of a stable hydrogen bonded connected water cage around the chemisorbed CO_2: this implies that whenever the Ni−CO_2 bond breaks, the solvent cage effect can enhance its recombination. To summarize, both molecular pictures of the NiNp and of the Ni slab consistently suggest that water molecules are prone to forming hydrogen bonds among themselves, rather than coordinating all of the interfacial Ni metal sites.

Our atomistic simulation results offer a different picture of the physicochemical behavior of NiNP in bulk water solution, compared to those previously suggested in the literature based on simple gas adsorption experiments/simulations on metal surfaces. To the best of our knowledge and probably motivated by the computational cost in modeling liquid water/metallic surfaces,[41] previous computational studies in literature have been focused only to the gas-phase CO_2 or to the adsorption of a very limited number of water molecules on selected Ni surfaces.[32−34,39] Our results indicate that, in bulk solution, NiNPs are incapable of coordinating too many water molecules: water coordination implies a decrease of the total NiNp charge (i.e., more and more negative), as the result of an electron withdrawing from the oxygen lone pair to the Ni cluster. For water and CO_2 adsorption on the 111 Ni surface, we observe the same behavior: upon water detachment from the slab interface, an interfacial cluster of water get formed by hydrogen bond (HB), followed by an increment of the total charge of the metal substrate. Water detachment and water clustering are not peculiar to the 111 Ni interface, but it has been also observed on other Ni interfaces and 6 adsorbed water molecules.[39] We also note that the adsorption energy of a single water molecule on the 111 Ni interface is ∼−11 kcal/

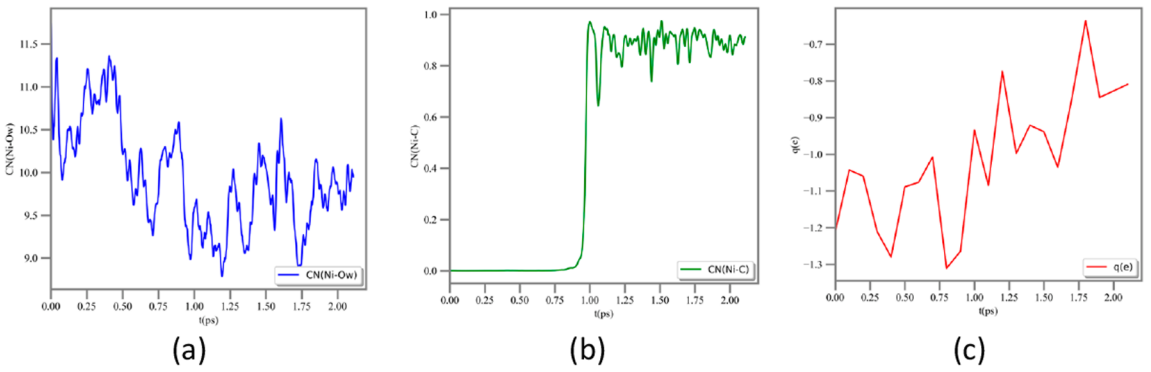

Figure 5. Ni−water oxygen (OW) coordination (a), Ni−carbon atom (C) coordination (b), and charge of the NiNP (c), over the first 2.2 ps of the FPMD at the PBE level.

https://doi.org/10.1021/acsomega.3c06676
ACS Omega 2024, 9, 771−780

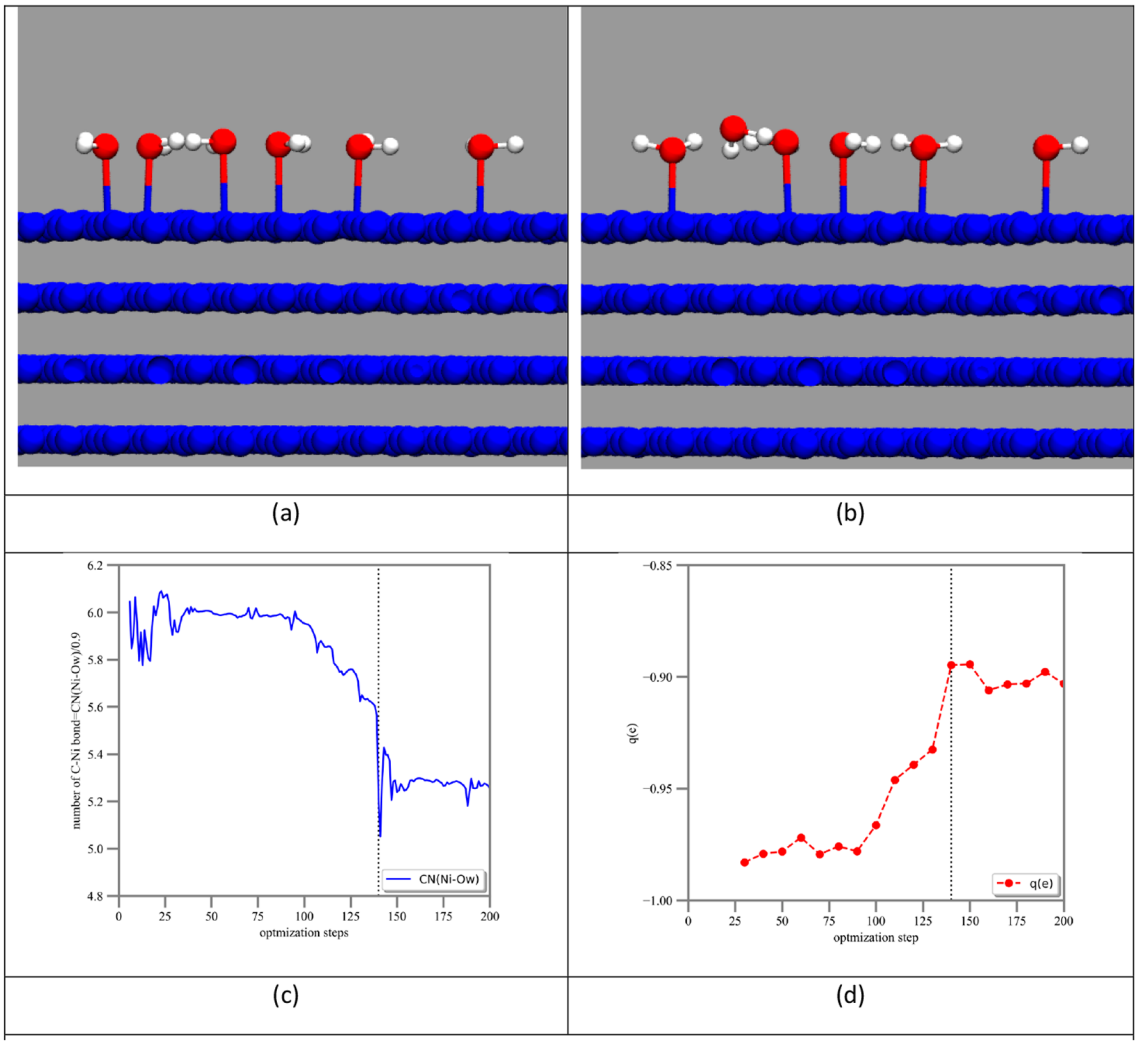

Figure 6. 111 Ni interface with 6 adsorbed water molecules. (a) Initial configuration and (b) after 200 geometry optimization steps. (c) Number of bonds, defined as the coordination number divided by 0.9 (see Methods), as a function of the optimization steps. (d) Mulliken charge of the Ni metal slab, as a function of the optimization step. Vertical dashed line indicates the transition with the decoordination of one water. Atom color code: O, red; Ni, blue; H, white.

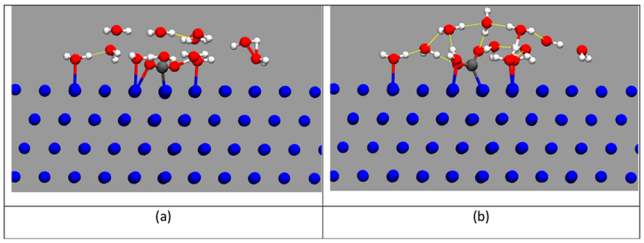

Figure 7. 111 Ni interface with 12 adsorbed water molecules and 1 CO_2. (a) Initial configuration and (b) after 200 geometry optimization steps. In yellow is the hydrogen bond network (cutoff distance = 0.35 nm, and cutoff angle = 30°). Atom color code: O, red; Ni, blue; H, white.

mol (Figure S3a), a value that agrees with those previously reported in the literature for different Ni surfaces.[33,34] The hydrogen bond energy in water ranges, depending on the type of environment (e.g., on ice, bulk water, on solid substrate, etc.), between 3 and 8 kcal/mol,[59] making the water decoordination from the Ni surface, and subsequent HB bond clustering, energetically feasible and entropically favorable in bulk solution.

We note that, upon hydration and CO_2 chemisorption, the total charge of the NiNP increases (i.e., less negative) as a result of both the water decoordination and a charge transfer from the NiNP to CO_2. This propensity of the metal Ni surface to coordinate electron withdrawing species is also supported by experimental literature showing monovalent cations or cationic polymer coordination on NiNP sites[38] and by computational and experimental studies showing the feasibility of gas-phase CO_2 adsorption on the Ni surface.[32,34,50,60] In the gas-phase adsorption of CO_2 on the Ni surface, CO_2 is adsorbed in a bent state, with an electron transfer from the Ni to the antibonding orbital of carbon dioxide.[34] We remark that, even if the gaseous CO_2 binding on the Ni surface is weak (see ref 34 and Figure S3b), The Ni–CO_2 bond stability can be favored by water caging around the chemisorbed molecule.[61] To summarize, the molecular picture coming out from this work suggests that NiNPs are not able to coordinate too many water molecules, leaving vacant sites that can be coordinated by electron withdrawing species, such as carbon dioxide or ions.

https://doi.org/10.1021/acsomega.3c06676
ACS Omega 2024, 9, 771−780

Our findings have profound implications on the molecular picture by which NiNP works in solutions. We here suggest that when CO_2 started to be sparged into the bulk solution, the formation of a NiNP surface highly decorated with hydroxyl groups (steps 1 and 2 in Figure 1) can be hampered by coordination of CO_2 (or cations if present) on the surface (steps 5 and 6 in Figure 1). Steps 5 and 6 have not been considered before in the previously suggested mechanism in literature.[27] The deactivation of the catalyst surface likely explains why, after an initial small boost of the hydration reaction represented by an increase of hydronium ions in solution (Figure 2b) and dissolved CO_2 (Figure 3), the catalytic action of the NiNPs in solutions rapidly vanish. The catalytic effects of the NiNPs previously reported was much more marked, and it may be ascribed to their different pH conditions (pH between 5.5 and 6.5) in which the experiments were performed.[27] The catalytic effect of NiNPs on carbon dioxide hydration, at least under our experimental conditions, was very modest. The same conclusions hold without the initial addition of NaOH. Finally, we want to highlight some potential technical issues associated with the use of NiNPs: the leaching of Ni^{2+} in solution, which may result in the presence of nickel in carbonate products, NiNPs aggregation, and the impossibility of using magnetic stirring (NiNPs are magnetic). These technical problems, together with a modest catalytic performance, depicted a scenario where NiNPs might not be an ideal candidate for large scale applications, unless their immobilization on inert substrates[42,43] could overcome some of these problems.

CONCLUSIONS

Carbon capture and utilization (CCU) certainty represents an appealing way to mitigate greenhouse gas levels in the atmosphere and to convert waste emissions in added-value products. The majority of CCU technologies rely on the dissolution of carbon dioxide in solution, i.e., its hydration from carbon dioxide into bicarbonate. Nickel nanoparticles have been suggested to catalyze the hydration of carbon dioxide in aqueous solutions, but the effectiveness of this has been questioned in literature.

To address the need for improving CCU at the industrial scale, we conducted a combined experimental and computational study aiming to shed light on the molecular mechanism and effectiveness by which NiNP may catalyze CO_2 hydration. Our results suggest that NiNPs have a modest effect in catalyzing such reaction, revealing an alternative chemical pathway (compared to that present in literature) about the NiNP behaviors in solutions. Water coordination on the metal surface causes an electron drag from oxygen's lone pair to the Ni surface, limiting the number of interfacial hydroxyl groups prone to CO_2 coordination and hydration, leaving vacant sites for the coordination of electron withdrawing species such as cations and carbon dioxide. This will cause deactivation of the surface of the catalyst. Thus, while NiNPs may accelerate CO_2 hydration in water restricted conditions (e.g., water vapor deposition on Ni surface), this catalytic effect seems limited in fully hydrated conditions. Some experimental technical issues (i.e., Ni^{2+} leaching, NiNP aggregation, and NiNP magnetic character) together with the limited catalytic activity here reported may hamper the large scale application of NiNPs, unless their immobilization on substrates may resolve some of the issues highlighted in this work.

ASSOCIATED CONTENT

Supporting Information

The Supporting Information is available free of charge at https://pubs.acs.org/doi/10.1021/acsomega.3c06676.

Schematic picture of the experimental apparatus (Figure S1), optimized icosahedral NiNp structure (Figure S2), single CO_2 and H_2O adsorption on Ni(111) surface (Figure S3), experimental pH time series (Figure S4), reaction rate from variation of the hydronium concentration (Figure S5), pH time series without NaOH addition (Figure S6), snapshot and results from FPMD at RPBE level (Figures S7 and S8) (PDF)

AUTHOR INFORMATION

Corresponding Authors

Alessandro Sinopoli − *Qatar Environment and Energy Research Institute, Hamad Bin Khalifa University, Doha, Qatar*; orcid.org/0000-0001-7993-4268; Email: asinopoli@hbku.edu.qa

Ivan Gladich − *Qatar Environment and Energy Research Institute, Hamad Bin Khalifa University, Doha, Qatar*; orcid.org/0000-0003-0929-3439; Email: igladich@hbku.edu.qa

Authors

Ziao Liu − *Department of Earth and Environmental Science and Department of Chemistry, University of Pennsylvania, Philadelphia, Pennsylvania 19104, United States*; orcid.org/0000-0002-0271-5101

Ahmed Abotaleb − *Qatar Environment and Energy Research Institute, Hamad Bin Khalifa University, Doha, Qatar*

Alaa Alkhateeb − *Qatar Environment and Energy Research Institute, Hamad Bin Khalifa University, Doha, Qatar*

Complete contact information is available at: https://pubs.acs.org/10.1021/acsomega.3c06676

Notes

The authors declare no competing financial interest.

ACKNOWLEDGMENTS

For HPC resources and services, we acknowledge the Research Computing group in Texas A&M University at Qatar, founded by the Qatar Foundation for Education, Science and Community Development, and the use of Qatar Environment and Energy Research Institute (QEERI) HPC under Project ID HPC-P21003. We thank Dr. Mohamed Madjet and Prof. Ali Kachmar for useful discussions on the computational setup. We acknowledge Prof. Joseph S. Francisco for useful discussion and comments.

REFERENCES

(1) Shakun, J. D.; Clark, P. U.; He, F.; Marcott, S. A.; Mix, A. C.; Liu, Z.; Otto-Bliesner, B.; Schmittner, A.; Bard, E. Global warming preceded by increasing carbon dioxide concentrations during the last deglaciation. *Nature* **2012**, *484* (7392), 49−54.

(2) Metz, B.; Davidson, O.; de Coninck, H.; Loos, M.; Meyer, L. *IPCC Special Report on Carbon Dioxide Capture and Storage*; Intergovernmental Panel on Climate Change (IPCC), 2005.

(3) Horowitz, C. A. Paris Agreement. *International Legal Materials* **2016**, *55* (4), 740−755.

(4) Rochelle, G. T. Amine Scrubbing for CO_2 Capture. *Science* **2009**, *325* (5948), 1652.

(5) Pan, Z. J.; Yang, R. T. Catalytic behavior of transition metal oxide in graphite gasification by oxygen, water, and carbon dioxide. *J. Catal.* **1991**, *130* (1), 161−172.
(6) Trachtenberg, M. C.; Bao, L.; Goldman, S. L.; Smith, D. A.; Wu, X. Flue gas CO_2 capture by a green liquid membrane. In *Greenhouse Gas Control Technologies 7*; Rubin, E. S., Keith, D. W., Gilboy, C. F., Wilson, M., Morris, T., Gale, J.; Thambimuthu, K., Eds.; Elsevier Science: Oxford, U.K., 2005; Vol. *II*, Part 2, pp 1751−1754. DOI: 10.1016/B978-008044704-9/50205-6.
(7) Markewitz, P.; Kuckshinrichs, W.; Leitner, W.; Linssen, J.; Zapp, P.; Bongartz, R.; Schreiber, A.; Müller, T. E. Worldwide innovations in the development of carbon capture technologies and the utilization of CO2. *Energy Environ. Sci.* **2012**, *5* (6), 7281−7305.
(8) Lackner, K. S. A Guide to CO2 Sequestration. *Science* **2003**, *300* (5626), 1677−1678.
(9) Dunsmore, H. E. A geological perspective on global warming and the possibility of carbon dioxide removal as calcium carbonate mineral. *Energy Conversion and Management* **1992**, *33* (5), 565−572.
(10) Pedersen, O.; Colmer, T.; Sand-Jensen, K. Underwater Photosynthesis of Submerged Plants - Recent Advances and Methods. *Front. Plant Sci.* **2013**, *4*, 140.
(11) McBain, J. W. LXXXV.—The use of phenolphthalein as an indicator. The slow rate of neutralisation of carbonic acid. *Journal of the Chemical Society, Transactions* **1912**, *101* (0), 814−820.
(12) Nguyen, M. T.; Matus, M. H.; Jackson, V. E.; Ngan, V. T.; Rustad, J. R.; Dixon, D. A. Mechanism of the Hydration of Carbon Dioxide: Direct Participation of H2O versus Microsolvation. *J. Phys. Chem. A* **2008**, *112* (41), 10386−10398.
(13) Adamczyk, K.; Prémont-Schwarz, M.; Pines, D.; Pines, E.; Nibbering, E. T. J. Real-Time Observation of Carbonic Acid Formation in Aqueous Solution. *Science* **2009**, *326* (5960), 1690−1694.
(14) Prabhu, C.; Wanjari, S.; Gawande, S.; Das, S.; Labhsetwar, N.; Kotwal, S.; Puri, A. K.; Satyanarayana, T.; Rayalu, S. Immobilization of carbonic anhydrase enriched microorganism on biopolymer based materials. *Journal of Molecular Catalysis B: Enzymatic* **2009**, *60* (1), 13−21.
(15) Wanjari, S.; Prabhu, C.; Yadav, R.; Satyanarayana, T.; Labhsetwar, N.; Rayalu, S. Immobilization of carbonic anhydrase on chitosan beads for enhanced carbonation reaction. *Process Biochemistry* **2011**, *46* (4), 1010−1018.
(16) Gladich, I.; Abotaleb, A.; Sinopoli, A. Tuning CO2 Capture at the Gas/Amine Solution Interface by Changing the Solvent Polarity. *J. Phys. Chem. B* **2020**, *124* (45), 10245−10256.
(17) Sinopoli, A.; Abotaleb, A.; Pietrucci, F.; Gladich, I. Stability of a Monoethanolamine-CO2 Zwitterion at the Vapor/Liquid Water Interface: Implications for Low Partial Pressure Carbon Capture Technologies. *J. Phys. Chem. B* **2021**, *125* (18), 4890−4897.
(18) Maginn, E. J. Virtual Issue on Carbon Dioxide: Physical Chemistry That Impacts Its Capture, Sequestration, and Conversion. *J. Phys. Chem. B* **2022**, *126* (48), 9927−9929.
(19) Sahoo, P. C.; Kumar, M.; Puri, S. K.; Ramakumar, S. S. V. Enzyme inspired complexes for industrial CO2 capture: Opportunities and challenges. *Journal of CO2 Utilization* **2018**, *24*, 419−429.
(20) Caplow, M. Bromine catalysis for carbon dioxide hydration and dehydration and some observations concerning the mechanism of carbonic anhydrase. *J. Am. Chem. Soc.* **1971**, *93* (1), 230−235.
(21) Huang, D.; Makhlynets, O. V.; Tan, L. L.; Lee, S. C.; Rybak-Akimova, E. V.; Holm, R. H. Kinetics and mechanistic analysis of an extremely rapid carbon dioxide fixation reaction. *Proc. Natl. Acad. Sci. U. S. A.* **2011**, *108*, 1222.
(22) Thee, H.; Smith, K. H.; da Silva, G.; Kentish, S. E.; Stevens, G. W. Carbonic anhydrase promoted absorption of CO2 into potassium carbonate solutions. *Greenhouse Gases: Science and Technology* **2015**, *5* (1), 108−114.
(23) Guo, D.; Thee, H.; da Silva, G.; Chen, J.; Fei, W.; Kentish, S.; Stevens, G. W. Borate-Catalyzed Carbon Dioxide Hydration via the Carbonic Anhydrase Mechanism. *Environ. Sci. Technol.* **2011**, *45* (11), 4802−4807.
(24) Verma, M.; Deshpande, P. A. Mechanistic insights into biomimetic carbonic anhydrase action catalyzed by doped carbon nanotubes and graphene. *Phys. Chem. Chem. Phys.* **2017**, *19* (13), 8757−8767.
(25) Zhang, N.; Santos, R. M.; Šiller, L. Rapid CO2 capture-to-mineralisation in a scalable reactor. *Reaction Chemistry & Engineering* **2020**, *5* (3), 473−484.
(26) Abotaleb, A.; Gladich, I.; Alkhateeb, A.; Mardini, N.; Bicer, Y.; Sinopoli, A. Chemical and physical systems for sour gas removal: An overview from reaction mechanisms to industrial implications. *Journal of Natural Gas Science and Engineering* **2022**, *106*, 104755.
(27) Bhaduri, G. A.; Šiller, L. Nickel nanoparticles catalyse reversible hydration of carbon dioxide for mineralization carbon capture and storage. *Catalysis Science & Technology* **2013**, *3* (5), 1234−1239.
(28) Bhaduri, G. A.; Alamiry, M. A. H.; Šiller, L. Nickel Nanoparticles for Enhancing Carbon Capture. *J. Nanomater.* **2015**, *2015*, 1−13.
(29) Bhaduri, G. A.; Šiller, L. Nickel nanoparticles catalyse reversible hydration of carbon dioxide for mineralization carbon capture and storage. *Catal. Sci. Technol.* **2013**, *3* (5), 1234.
(30) Zhang, N.; Santos, R. M.; Smith, S. M.; Šiller, L. Acceleration of CO_2 mineralisation of alkaline brines with nickel nanoparticles catalysts in continuous tubular reactor. *Chem. Eng. J.* **2019**, *377*, 120479.
(31) Huang, D.; Makhlynets, O. V.; Tan, L. L.; Lee, S. C.; Rybak-Akimova, E. V.; Holm, R. H. Kinetics and mechanistic analysis of an extremely rapid carbon dioxide fixation reaction. *Proc. Natl. Acad. Sci. U. S. A.* **2011**, *108* (4), 1222.
(32) Cai, J.; Han, Y.; Chen, S.; Crumlin, E. J.; Yang, B.; Li, Y.; Liu, Z. CO2 Activation on Ni(111) and Ni(100) Surfaces in the Presence of H2O: An Ambient-Pressure X-ray Photoelectron Spectroscopy Study. *J. Phys. Chem. C* **2019**, *123* (19), 12176−12182.
(33) Mohsenzadeh, A.; Bolton, K.; Richards, T. DFT study of the adsorption and dissociation of water on Ni(111), Ni(110) and Ni(100) surfaces. *Surf. Sci.* **2014**, *627*, 1−10.
(34) Wang, S.-G.; Cao, D.-B.; Li, Y.-W.; Wang, J.; Jiao, H. Chemisorption of CO2 on Nickel Surfaces. *J. Phys. Chem. B* **2005**, *109* (40), 18956−18963.
(35) Ramsden, J. J.; Sokolov, I. J.; Malik, D. J. Questioning the catalytic effect of Ni nanoparticles on CO2 hydration and the very need of such catalysis for CO2 capture by mineralization from aqueous solution. *Chem. Eng. Sci.* **2018**, *175*, 162−167.
(36) Bhaduri, G. A.; Šiller, L. Comment on "Questioning the catalytic effect of Ni nanoparticles on CO2 hydration and the very need of such catalysis for CO2 mineralization from aqueous solutions by Ramsden et al. Chem. Eng. Sci.(2018) 175−162. *Chem. Eng. Sci.* **2019**, *195*, 1029−1030.
(37) Bodor, M.; Santos, R. M.; Chiang, Y. W.; Vlad, M.; Van Gerven, T. Impacts of nickel nanoparticles on mineral carbonation. *Sci. World J.* **2014**, *2014*, 921974.
(38) Seo, S.; Perez, G. A.; Tewari, K.; Comas, X.; Kim, M. Catalytic activity of nickel nanoparticles stabilized by adsorbing polymers for enhanced carbon sequestration. *Sci. Rep.* **2018**, *8* (1), 11786.
(39) Zhu, L.; Liu, C.; Wen, X.; Li, Y.-W.; Jiao, H. Coverage-Dependent Water Dissociative Adsorption Properties on Nickel Surfaces. *J. Phys. Chem. C* **2020**, *124* (47), 25835−25845.
(40) Gong, L.; Chen, J.-J.; Mu, Y. Catalytic CO2 reduction to valuable chemicals using NiFe-based nanoclusters: a first-principles theoretical evaluation. *Phys. Chem. Chem. Phys.* **2017**, *19* (41), 28344−28353.
(41) Groß, A.; Sakong, S. Ab Initio Simulations of Water/Metal Interfaces. *Chem. Rev.* **2022**, *122* (12), 10746−10776.
(42) Han, X.; Williamson, F.; Bhaduri, G. A.; Harvey, A.; Šiller, L. Synthesis and characterisation of ambient pressure dried composites of silica aerogel matrix and embedded nickel nanoparticles. *Journal of Supercritical Fluids* **2015**, *106*, 140−144.
(43) Hassan, K. T.; Wang, J.; Han, X.; Sharp, J. J.; Bhaduri, G. A.; Martis, V.; Šiller, L. Catalytic Performance of Nickel Nanowires

Immobilized in Silica Aerogels for the CO2 Hydration Reaction. *ACS Omega* **2019**, *4* (1), 1824−1830.
(44) Gordon, M. B.; Cyrot-Lackmann, F.; Desjonquères, M. C. Relaxation and stability of small transition metal particles. *Surf. Sci.* **1979**, *80*, 159−164.
(45) Jain, A.; Ong, S. P.; Hautier, G.; Chen, W.; Richards, W. D.; Dacek, S.; Cholia, S.; Gunter, D.; Skinner, D.; Ceder, G.; Persson, K. A. Commentary: The Materials Project: A materials genome approach to accelerating materials innovation. *APL Mater.* **2013**, *1* (1), 011002.
(46) The Materials, P., *Materials Data on Ni by Materials Project*; Lawrence Berkeley National Laboratory, 2020.
(47) Mittendorfer, F.; Eichler, A.; Hafner, J. Structural, electronic and magnetic properties of nickel surfaces. *Surf. Sci.* **1999**, *423* (1), 1−11.
(48) Perdew, J. P.; Ruzsinszky, A.; Csonka, G. I.; Vydrov, O. A.; Scuseria, G. E.; Constantin, L. A.; Zhou, X.; Burke, K. Restoring the Density-Gradient Expansion for Exchange in Solids and Surfaces. *Phys. Rev. Lett.* **2008**, *100* (13), 136406.
(49) Perdew, J. P.; Burke, K.; Ernzerhof, M. Generalized Gradient Approximation Made Simple. *Phys. Rev. Lett.* **1996**, *77* (18), 3865−3868.
(50) Hammer, B.; Hansen, L. B.; Nørskov, J. K. Improved adsorption energetics within density-functional theory using revised Perdew-Burke-Ernzerhof functionals. *Phys. Rev. B* **1999**, *59* (11), 7413−7421.
(51) Grimme, S.; Antony, J.; Ehrlich, S.; Krieg, H. A consistent and accurate ab initio parametrization of density functional dispersion correction (DFT-D) for the 94 elements H-Pu. *J. Chem. Phys.* **2010**, *132* (15), 154104.
(52) Goedecker, S.; Teter, M.; Hutter, J. Separable dual-space Gaussian pseudopotentials. *Phys. Rev. B* **1996**, *54* (3), 1703−1710.
(53) Martyna, G. J.; Klein, M. L.; Tuckerman, M. Nosé-Hoover chains: The canonical ensemble via continuous dynamics. *J. Chem. Phys.* **1992**, *97* (4), 2635−2643.
(54) Hutter, J.; Iannuzzi, M.; Schiffmann, F.; VandeVondele, J. cp2k: atomistic simulations of condensed matter systems. *Wiley Interdisciplinary Reviews: Computational Molecular Science* **2014**, *4* (1), 15−25.
(55) Bonomi, M.; Bussi, G.; Camilloni, C.; Tribello, G. A.; Banáš, P.; Barducci, A.; Bernetti, M.; Bolhuis, P. G.; Bottaro, S.; Branduardi, D.; Capelli, R.; Carloni, P.; Ceriotti, M.; Cesari, A.; Chen, H.; Chen, W.; Colizzi, F.; De, S.; De La Pierre, M.; Donadio, D.; Drobot, V.; Ensing, B.; Ferguson, A. L.; Filizola, M.; Fraser, J. S.; Fu, H.; Gasparotto, P.; Gervasio, F. L.; Giberti, F.; Gil-Ley, A.; Giorgino, T.; Heller, G. T.; Hocky, G. M.; Iannuzzi, M.; Invernizzi, M.; Jelfs, K. E.; Jussupow, A.; Kirilin, E.; Laio, A.; Limongelli, V.; Lindorff-Larsen, K.; Löhr, T.; Marinelli, F.; Martin-Samos, L.; Masetti, M.; Meyer, R.; Michaelides, A.; Molteni, C.; Morishita, T.; Nava, M.; Paissoni, C.; Papaleo, E.; Parrinello, M.; Pfaendtner, J.; Piaggi, P.; Piccini, G.; Pietropaolo, A.; Pietrucci, F.; Pipolo, S.; Provasi, D.; Quigley, D.; Raiteri, P.; Raniolo, S.; Rydzewski, J.; Salvalaglio, M.; Sosso, G. C.; Spiwok, V.; Šponer, J.; Swenson, D. W. H.; Tiwary, P.; Valsson, O.; Vendruscolo, M.; Voth, G. A.; White, A. Promoting transparency and reproducibility in enhanced molecular simulations. *Nat. Methods* **2019**, *16* (8), 670−673.
(56) Lindskog, S.; Coleman, J. E. The Catalytic Mechanism of Carbonic Anhydrase. *Proc. Natl. Acad. Sci. U. S. A.* **1973**, *70* (9), 2505−2508.
(57) König, M.; Vaes, J.; Klemm, E.; Pant, D. Solvents and Supporting Electrolytes in the Electrocatalytic Reduction of CO2. *iScience* **2019**, *19*, 135−160.
(58) Li, J.; Guo, J.; Dai, H. Probing dissolved CO2(aq) in aqueous solutions for CO2 electroreduction and storage. *Sci. Adv.* **2022**, *8* (19), eabo0399.
(59) Huš, M.; Urbic, T. Strength of hydrogen bonds of water depends on local environment. *J. Chem. Phys.* **2012**, *136* (14), eabo0399.
(60) Vogt, C.; Groeneveld, E.; Kamsma, G.; Nachtegaal, M.; Lu, L.; Kiely, C. J.; Berben, P. H.; Meirer, F.; Weckhuysen, B. M. Unravelling structure sensitivity in CO2 hydrogenation over nickel. *Nature Catalysis* **2018**, *1* (2), 127−134.
(61) Nissenson, P.; Knox, C. J. H.; Finlayson-Pitts, B. J.; Phillips, L. F.; Dabdub, D. Enhanced photolysis in aerosols: evidence for important surface effects. *Phys. Chem. Chem. Phys.* **2006**, *8* (40), 4700−4710.

https://doi.org/10.1021/acsomega.3c06676
ACS Omega 2024, 9, 771−780